NOVEL APPROACH TO DETERMINE THE YOUNG'S MODULUS IN SILICON-ON-INSULATOR WAVEGUIDE USING MICRORING RESONATOR

M. BAHADORAN[*], M.S. AZIZ, A. F. A. NOORDEN, M. A. JALIL[a], J. ALI, P. P. YUPAPIN[b]
Institute of Advanced Photonics Science, Nanotechnology Research Alliance Universiti Teknologi Malaysia (UTM), 81310 Johor Bahru, Malaysia
[a]Department of Physics, Faculty of Science, Universiti Teknologi Malaysia (UTM), 81310 Johor Bahru, Malaysia
[b]Nanoscale Science and Engineering Research Alliance (N'SERA), Faculty of Science King Mongkut's Institute of Technology Ladkrabang (KMITL), Bangkok 10520, Thailand

A novel approach using microresonating system with low power consumption is proposed for determining Young's modulus of mirco and nano-sized waveguide material. Based on the Mason rule with signal flow graph (SFG) method in the Z-domain, the optical transfer function is derived for resonating layout consists of two single microring resonators which are indirectly coupled to an add-drop micro resonator. A mathematical function is determined for critical coupling coefficient and the optimum optical transmission of proposed system. For the resonant mode numbers of 5;3;3, the free spectral range (FSR) is extended to 182 nm with the out of band rejection ratio(OBRR) of 50 dB and the Q factor is 8593 .The Young's modulus is determined based on a change in the sensing ring radius due to the applied external force on the waveguide that causes the wavelength shift in resonant peaks. The Young's modulus for the lateral surface of the SOI waveguide with 250 nm height and 1.5μm radius is determined to be 147.72 GPa and for the upper surface of the SOI waveguide with 440 nm average width and 1.5μm radius is determined to be 83.93 GPa. The proposed resonating system is a potential candidate for measuring Young's modulus of materials in mirco and nano size with high resolution and has the advantages of the low power consumption due to the low intensity source.

1. Introduction

The Young's modulus is known as one of the important material properties in engineering, material science, and sensors which describes the degree of deformation resistance of a material under the applied force [1]. The Young's modulus is closely related to the internal structure of solid at the atomics and microstructural level and has become one of the key courses in material science[2]. Nowadays, there are various applications which focus on measuring the Young's modulus of materials such as mechanobiological models in tissue engineering [3], stress transfer in nanocomposite [4], molecules binding [5], biosensor [6], and high-sensitive force sensor [7].

In this paper we focus on using the waveguide based evanescent field sensors which have received great interest due to their low cost, high-sensitivity and suitability for implementing into an array format [8]. For a ring-based Vernier sensor an small perturbation in waveguide length will introduce a significant wavelength shift that result in a shift of resonant peak and provides a ultra-high sensitivity[9, 10]. In this manuscript, the Mason's rule [11-13] with signal flow graph (SFG) method [14] in the Z-domain is applied to drive the optical transfer function for a silicon-on-insulator (SOI) resonating system. The Vernier effect [15, 16] is used for SOI microring configuration consist of two single ring resonators which are indirectly coupled with an add-drop

---

[*] Corresponding author: bahadoran@utm.my

resonator to obtained an extended free spectrum range (FSR) with high Q factor and sharp resonant peaks. In practice, the proposed system is worked by means of the change of a ring radius due to a load cell or other physical parameters, in which the sensing and reference signals are analyzed, simulated and compared to form the measurement. Based on the wavelength sensing interrogation [17], the Young's modulus for SOI waveguide is determined. Our proposed technique is suitable for measuring Young's modulus of waveguide materials in mirco and nano size with high resolution and has the advantages of the low power consumption due to the low intensity source.

2. Analysis

A micro resonating layout consists of two single ring resonators which are vertically coupled with an add-drop resonator with 2×2 optical couplers is shown in Fig. 1.a. The rings are considered to couple indirectly together as each bus waveguide used in common for two microring resonators. The SFG diagram of 2×2 optical directional couplers is illustrated in Fig.1.b. By taking into account the insertion loss γ for each coupling region and the coupling factor k_i of the ith coupler (Here after 1 and 2 indices show the quantities belong to the add-drop resonator while R and S indices show the quantities belong to reference and sensor units, respectively), the fraction of light pass through the throughput path is expressed as $C_i = \sqrt{(1-\gamma_i)(1-k_i)}$ [18] and in contrast, the fraction of light pass through the cross path is expressed as $S_i = \sqrt{(1-\gamma_i)k_i}$ [19-21]. The transmission of light along the ring resonator is considered as the Z-transform parameter and defined as $Z^{-1} = \exp(-j 2\pi n_{eff} L / \lambda)$. Here n_{eff} is the effective refractive index of the waveguide, λ is the signal's center wavelength and the ring's circumference is $L = 2\pi R$, which R shows the radius of the ring resonator. The free spectral range (FSR) of the device is determined by $FSR = c/n_g L$ where $n_g = n_{eff} + f_0 (dn_{eff}/df)_{f_0}$ is the group refractive index of the ring, n_{eff} is the effective refractive index, and f_0 is the design (center) frequency[9] [22]. The optical transfer function, H, for an optical device with the input photonics node $E_i(z)$ and the output photonics node $E_n(z)$ is given by Mason rule [13, 23]

$$H = \frac{E_n(z)}{E_i(z)} = \frac{1}{\Delta} \sum_{j=1}^{n} T_j \Delta_j \tag{1}$$

where T_j shows the gain of the ith onward path from the input to output port and n is the overall number of onward paths from input to output photonics nodes. The symbol Δ_j considers all of the loops that remain untouched while a signal transverses via each T_j forward path from input to output photonics nodes. The signal flow graph determinant is displayed by Δ , which is given by[24, 25]

$$\Delta = 1 - \sum_{i=1} L_i + \sum_{i \neq j} L_i \ L_i - \sum_{i \neq j \neq k} L_i \ L_j L_k + ... \tag{2}$$

here L_i is the transmittance gain of the ith loop. The SFG for our proposed system illustrated in Fig. 1.b, in which the input photonics node is $E_2=E_{in}$ and $E_5=E_{drop}$ is considered as the drop photonics node. The FSR of the vertically coupled ring resonator with different radii can be determined by [26] [27]

$$FSR_{tot} = N_1.FSR_1 = N_R.FSR_R = N_S.FSR_S \tag{3}$$

where N_1 , N_R , and N_S are representing the resonant mode numbers (RMNs) for add-drop, reference and sensor microresonating units, respectively. All of these RMNs should be integer and coprime. Based on Eq.(1) the optical transfer function for through and drop ports of proposed

system can be written as $H_{82}^{thr} = E_8(z)/E_2(z)$ and $H_{52}^{drp} = E_5(z)/E_2(z)$ in which $E_8(z)$, $E_5(z)$ and $E_2(z)$ are considered as the through , drop and input photonics nodes, respectively. Identifying all loop gains from SFG diagram is the first step in determining the OTF for both through and drop ports. Totally, six loop gains can be found in the proposed system that three of them are independent loops as

$$L_1 = L_R = C_R \; \xi_R^{NR} \tag{4}$$

$$L_1 = C_1 C_2 \; \xi_1^{N1} \tag{5}$$

$$L_3 = L_S = C_S \; \xi_S^{NS} \tag{6}$$

For each microring resonator $\xi_q^N \equiv X_q Z^{-N}$ is defined as the multiplication of Z-transform parameter $Z^{-N} = \exp(-j\varphi N)$ times a roundtrip loss coefficient $X_q = \exp(-\alpha L_q/2)$. Here $\varphi = k\, n_{eff}\, L$ is phase shift [28] and N defines as integer resonant numbers of each ring in the system, α is the intensity attenuation coefficient of the waveguide and L_q shows the circumference of each ring. As shown in Fig.1.b four non-touching loops from multiplication of separate loops can be identify as

$$L_4 = L_1.L_R = C_1 C_2 \; C_R \, \xi_R^{NR} \, \xi_1^{N1} \tag{7}$$

$$L_5 = L_1.L_S = C_1 C_2 \; C_S \, \xi_S^{NS} \, \xi_1^{N1} \tag{8}$$

$$L_6 = L_R.L_S = C_S C_R \; \xi_S^{NS} \, \xi_R^{NR} \tag{9}$$

The second step in determining OTF is recognizing all of the forward transmitting paths, T_j, and their SFG determinant, Δ_j, from input to output photonics nodes. Three forward transmitting paths can be identified from input photonics node, 2, to the through port photonics node ,8,. The first forward transmitting direction, T_1^{thr}, sweeps the system's reference unit via photonics nodes of $2 \rightarrow 7 \rightarrow 1 \rightarrow 8$ as

$$T_1^{thr} = -\; S_R^2 \; \xi_R^{NR} \tag{10}$$

The SGF determinant for the first path is

$$\Delta_1^{thr} = 1 - L_1 - L_S + L_1 L_S \tag{11}$$

The second forward path transmittance touches the add-drop resonator from photonics nodes of $2 \rightarrow 9 \rightarrow 10 \rightarrow 4 \rightarrow 3 \rightarrow 8$ and the is given by

$$T_2^{thr} = -\; S_1^2 \; C_2 \, \xi_1^{N1} \tag{12}$$

and the SGF determinant for this route is

$$\Delta_2^{thr} = 1 - L_R - L_S + L_R L_S \tag{13}$$

The third forward track passes directly from input node, 2, to through put node, 8, and is given by

$$T_3^{thr} = C_1 C_R \tag{14}$$

As this route does not touch any loops, the SGF determinant becomes

$$\Delta_1^{thr} = 1 - L_1 - L_R - L_S + L_1 L_R + $$
$$L_R L_S + L_1 L_S - L_1 L_S L_R \tag{15}$$

The optical transfer function for the through port of proposed resonating system is calculated by substituting Eqs. (4) till (9) into Eq.(2) and Eqs. (10) till Eq.(15) into Eq.(1),

$$H_{82}^{thr} = \frac{\begin{aligned} &\{C_1 C_R - C_1 C_R C_S \xi_S^{NS} + [C_S \xi_S^{NS} - 1] \times \\ &[\xi_R^{NR}(S_R^2 + C_1 C_R^2) + C_2 \xi_1^{N1}(S_1^2 + C_R C_1^2) - \\ &C_2 \xi_1^{N1} \xi_R^{NR}(C_1 S_R^2 + C_R S_1^2 + C_R^2 C_1^2)]\} \end{aligned}}{\begin{aligned} &\{1 - C_R \xi_R^{NR} - C_1 C_2 \xi_1^{N1} - C_S \xi_S^{NS} + C_1 C_2 \times \\ &C_R \xi_R^{NR} \xi_1^{N1} + C_S C_R \xi_R^{NR} \xi_S^{NS} + C_1 C_2 C_S \times \\ &\xi_1^{N1} \xi_S^{NS} - C_1 C_2 C_R C_S \xi_1^{N1} \xi_R^{NR} \xi_S^{NS}\} \end{aligned}} \tag{18}$$

To determine the OTF for the drop port of resonating system, all of the tracks from the input photonics node ,2, to the drop port photonics node ,8, should also be identified. As shown in Fig. 1.b merely one onward transmitting route can be found which touches the photonics nodes of $2 \rightarrow 9 \rightarrow 10 \rightarrow 5$. Thus the drop transmitting path is

$$T_1^{drp} = - S_1 S_2 \sqrt{\xi_1^{N1}} \tag{19}$$

The SGF determinant for this single path is

$$\Delta_1^{drp} = 1 - L_R - L_S + L_R L_S \tag{20}$$

replacing Eqs. (4-9) into Eq.(2) and Eqs. (19-20) into Eq.(1), then the optical transfer function for the drop port of proposed resonating system is

$$H_{82}^{drp} = \frac{\begin{aligned} &\{(-S_1 S_2 \sqrt{\xi_1^{N1}})(1 - C_R \xi_R^{NR} - \\ &C_S \xi_S^{NS} + C_R C_S \xi_R^{NR} \xi_S^{NS})\} \end{aligned}}{\begin{aligned} &\{1 - C_R \xi_R^{NR} - C_1 C_2 \xi_1^{N1} - C_S \xi_S^{NS} + C_1 C_2 \times \\ &C_R \xi_R^{NR} \xi_1^{N1} + C_S C_R \xi_R^{NR} \xi_S^{NS} + C_1 C_2 C_S \times \\ &\xi_1^{N1} \xi_S^{NS} - C_1 C_2 C_R C_S \xi_1^{N1} \xi_R^{NR} \xi_S^{NS}\} \end{aligned}} \tag{21}$$
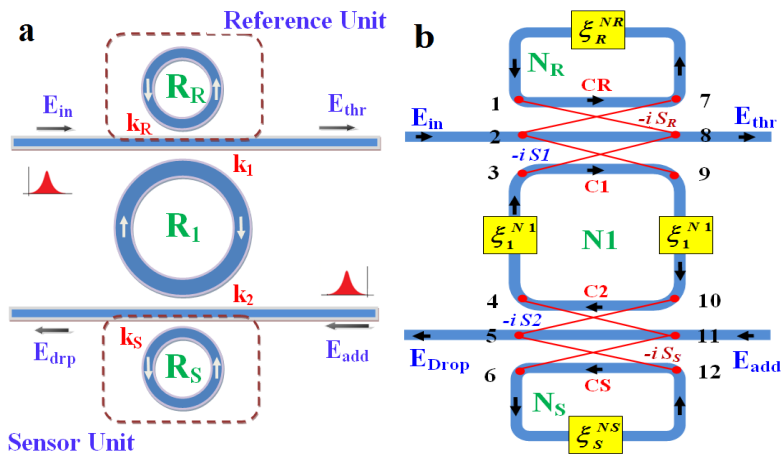
Fig. 1 Microring resonator configuration for force sensing. (a) waveguide layout and (b) Z-transform diagram SFG

3. Young's Modulus Determination

The high-index-contrast of silicon on insulator (SOI) enables to fabricate waveguides in sub-micrometer dimensions as well as microring resonators with radii of a few micrometers while ensuring low loss and single mode propagation [26]. The silicon on insulator(SOI) ring resonator with radius of $R_1=2.5$ µm [29] is used for add-drop resonator of our proposed resonating system. Two identical ring resonator are selected for reference and sensor units which have the same radii $R_R=R_S=1.5$ µm with the group refractive index of $n_g = 4.2$ and the effective mode core area around $A_{eff}=1.0$ µm² [30]. We suppose the same intensity insertion loss coefficients $\gamma = 0.01$ for the couplers between rings and the bus waveguides and also assume the same waveguide's intensity attenuation coefficient $\alpha = 20\,dBcm^{-1}$ for all rings. To obtain critical coupling from vanishing through port optical transfer function , $H_{82}^{thr} = 0$ [31], three assumption are considered as follow: using a similar coupling coefficients for bus waveguides with the reference and sensor units, $C_R = C_S$, selecting an identical coupling coefficients between the add-drop unit and the bus waveguides , $C_1 = C_2$, and for further simplification with considering the exponential series up to 1st order we suppose $\xi_1^{N1} = \xi_S^{NS} = \xi_R^{NR} \approx 1$ [16] which leads to

$$C_R = \frac{-C_1 \pm \sqrt{-C_1^6 + 3C_1^4 - 2C_1^2 + 1}}{C_1^3 - C_1^2 - C_1 + 1} \tag{22}$$

here $C_i = \sqrt{(1-\gamma)(1-k_i)}$ is the fraction of light passed through the integrated waveguide path and k_i is coupling coefficient. Based on the critical coupling relation in Eq.(22), for the coupling coefficients of $k_1 = k_2 = 0.01$ for the couplers between the add-drop resonator with bus waveguides, the symmetric coupling coefficients between bus waveguides and the reference unit and sensor unit are calculated to be $k_R = k_S = 0.90$. Based on Eq.(3), the resonant mode numbers for our proposed resonating system are $N_1=5$; $N_R=N_S=3$. As shown in Fig. 2, due to the Vernier effect the FSR from 62.5 nm for a microring resonator with radius of 1.5 µm[30] and 32 nm for radius of 2.5 µm [29] is extended to 182 nm for proposed microresonating configuration.
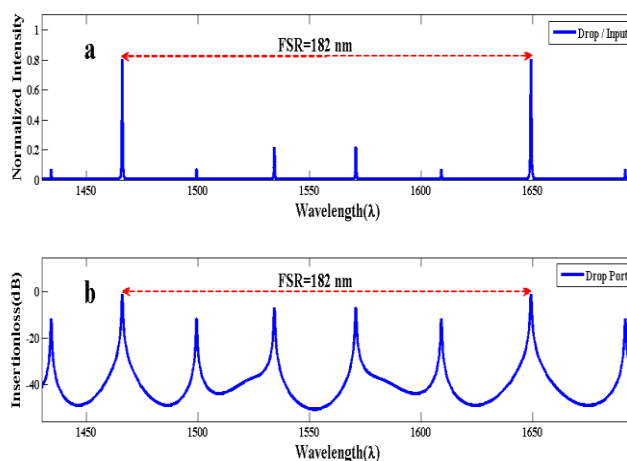
Fig. 2 *FSR enhancement due to the Vernier effect for proposed microresonating system with radii of $R_{add}=R_1=$ 2.5 µm; $R_S= R_R=$ 1.5 µm and the RMNs of ($N_1=$ 5, $N_R= N_S=$ 3) the coupling coefficients of $k_1= k_2=$ 0.01 and $k_R= k_S=$ 0.90. a) Normalized intensity. b) Insertion loss.*

Although achieving broaden FSR with a sharper peaks at resonances have been reported as the advantages of Vernier ring resonators[16, 32], but the resonances interval stop band area are suppressed and ignored. The suppression of the interstitial peaks brings about a decrease in the

resolution of optical devices for sensing applications as tracing of wavelength shifts are limited to the sharpness of resonant peaks. In order to intensify the stop band resonances, the coupling coefficients of $k_1 = k_2 = 0.01$ are selected for interferometer couplers between bus waveguides and the interferometer ring resonator, R_1, and an identical coupling coefficients of $k_R = k_S = 0.97$ are chosen for the couplers between bus waveguides with the reference and sensor units. As shown in Fig.3 for these set of coupling coefficients, the insertion loss in the resonant peaks and the interstitial peaks get almost the same values, thus in comparison with the determined critical coupling condition, the variation in the wavelength shift interval the resonant peaks can also be studied and the operating range of the proposed system is increased.

To determine the Young's modulus of SOI material in micro size, two identical SOI ring resonators with an equal radii of $R_S = R_R = 1500$ *nm* are used for the reference and the sensing rings. The sensing unit is surrounded in a medium and the applied force into sensing ring resonator can be in the form of distributed force within thin film material which is coated on the sensing unit, in which the excited thin film atom can be activated [9].
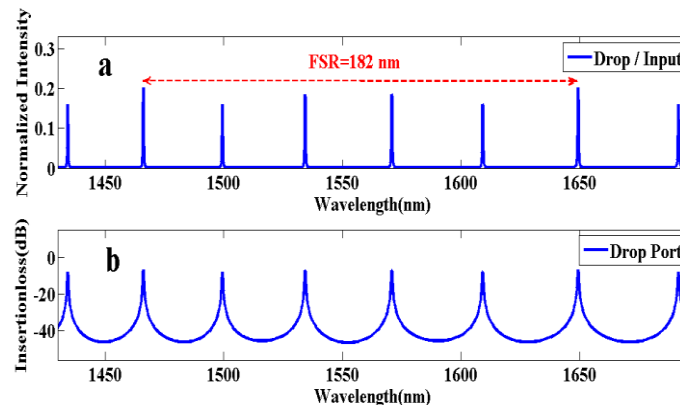
Fig.3: The amplification of the interstitial resonant peaks for proposed resonating system with the coupling coefficients of $k_1 = k_2 = 0.01$ and $k_R = k_S = 0.97$, radii of $R_1 = 2.5$ μm; $R_S = R_R = 1.5$ μm and the RMNs of $N_1 = 5$, $N_R = N_S = 3$ in the a) Normalized intensity b) Insertion loss.

The external force from the medium causes the variation of the ring's radius in the sensing unit. The add-drop resonator with the radius of $R_1 = 2500$ *nm* is used to form the interference signal between reference and sensing rings. In operation, the change in sensing ring radius is caused by the change in the shift of signals circulated in the interferometer ring (R_1), in which the interference signal is observed. The change in optical path length leads to form an interferometer system [9].

In simulation, the radial variation between 1 *nm* to 11 *nm* are assumed for the radius of the sensing ring resonator. It is assumed that two identical optical signals are fed into the input and add ports of optical system and the output signal from sensing and reference units are measured and compared. As shown in Fig. 4, the output signal from a system with an identical radii for reference and sensor units, $R_S = R_R = 1500$ *nm*, are considered as the sensor's base line. The wavelength shifts due to the change in sensing unit length for 1 *nm*, 3 *nm*, 5 *nm*, 9 *nm* and 11*nm* are shown in Fig.4. Based on the simulated results in Fig. 4.a and Fig.4.b, the resonant peaks interval extended FSR are shifted $\Delta\lambda = 0.3nm$ for the variation of $\Delta R = 1nm$ of the sensing unit ring radius. Simulated result in Fig. 4.c to Fig. 4.l show that, increase in the sensing unit length to 3 *nm*, 5 *nm*, 7 *nm*, 9 *nm* and 11 *nm* brings about the enhancements of the wavelength shift to 0.87*nm*, 1.45*nm*, 2.02*nm* and 3.17*nm*, respectively. It is assumed that the load cell or other sensing parameters can exert on the sensor unit, R_S, whereas stress and strain are introduced on the sensing device by mean of the elastic modulus of the materials, which is caused the difference in peak spectrum of both signals and described by [9, 33]

$$Y_0 = \left(\frac{F/A}{\Delta L/L}\right) = \frac{Stress}{Strain} \tag{23}$$

The relationship between force and the change in sensing unit length is described by

$$\Delta L = \left(\frac{F}{Y_0 A_0} \right) . L_0 \qquad (24)$$

where ΔL is the change in length of the sensing unit, F is the applied force, Y_0 is the Young's modulus, A_0 is the initial cross section area and L_0 is the initial length of the sensing unit.
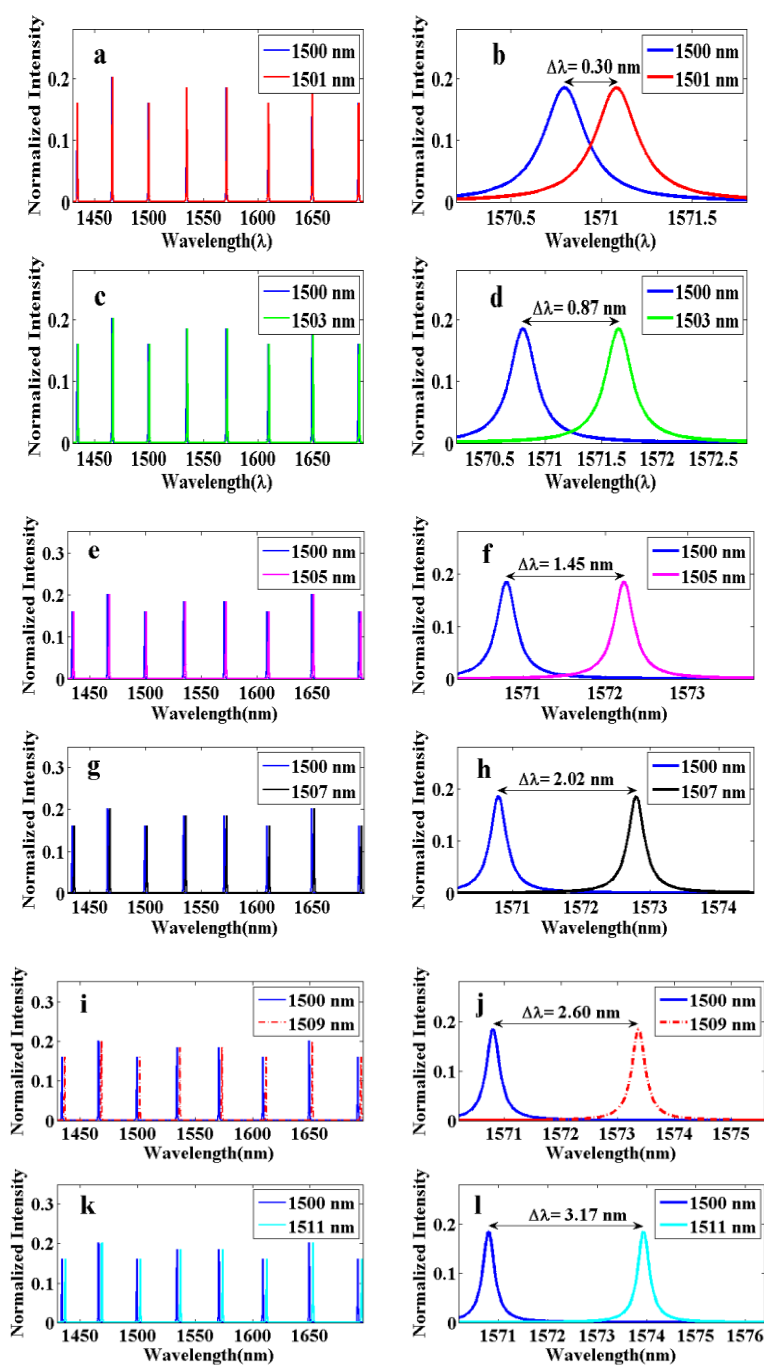
Fig. 4 The relationship between normalized intensity versus wavelength for reference unit with radius of 1500nm and the variation of the sensing unit ring radius for a- b) ΔR=1nm with wavelength shift of 0.3 nm. c-d) ΔR=3nm with wavelength shift of 0.87 nm. e-f) ΔR=5nm with wavelength shift of 1.45 nm. g-h) ΔR=7nm with wavelength shift of 2.02 nm. i- j) ΔR=9nm with wavelength shift of 2.60 nm. k-l) ΔR=11nm with wavelength shift of 3.17 nm.

The sensing line in Fig.5 is plotted based on the obtained wavelength shifts in Fig.4, which shows the linear relationship between the wavelength shift from the reference and sensing signals. Here a sensing range in terms of wavelength-shift ($\Delta\lambda$) within the resolution of 0.0 1 nm is achieved.
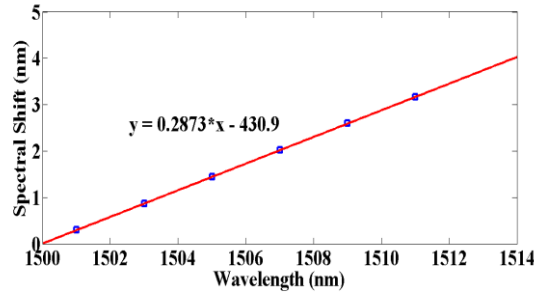
Fig. 5 Sensing line for determining Young's modulus of SOI waveguide.

Based on Eq. (24) and the slope of sensing line in Fig.5 is inversely proportional to the Young's modulus. The Young's modulus is determined for an ultra-compact silicon microring resonator with a radius of 1.5 μm, a height of 250 nm and an average width of ~ 440 nm, which is fabricated on a silicon-on-insulator substrate [30]. As shown in Fig.6, when external force is applied on the sensing ring with the width of 250 nm, the Young's modulus for the applied forces of 1nN, 10 μN and 0.1N are determined as 1477.23 Pa , 14.77 MPa and 147.72 Gpa, respectively. Change in the external forces direction from lateral side of the waveguide into the upper surface of the ring's waveguide with the width of 440 nm leads to Young's modulus of 839.37 Pa, 8.39 MPa and 83.93 Gpa, for the applied forces of 1nN, 10 μN and 0.1N, respectively. The determined Young's modulus from our proposed optical system for SOI waveguide material, with cross section of *250nm× 450nm,* are in the range of the reported Young's modulus for silicon (130-185GPa) and Young's modulus of silicon dioxide 72 GPa [34].
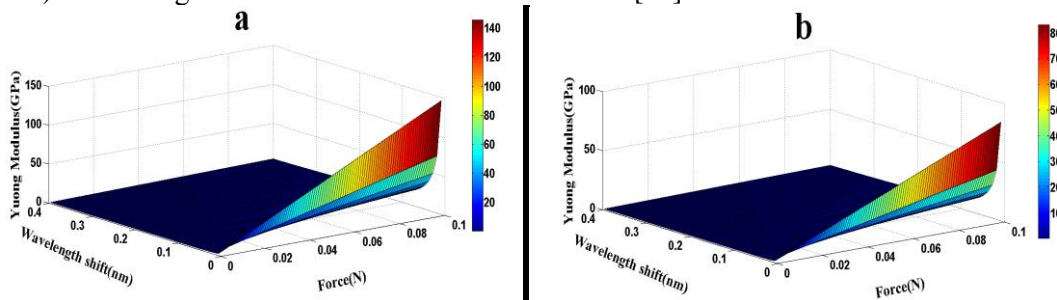
Fig.6 Young's modulus of SOI waveguide for a) The lateral surface of the sensing ring with the width of 250 nm. b) The top surface of the sensing ring with the width of 440 nm.

4. Conclusion

A novel approach using microresonating system with low power consumption is proposed for determining Young's modulus of mirco-sized waveguide material. The Vernier effect is applied for a photonics circuits consist of two single microring resonators which are indirectly coupled to add-drop micro resonator from SOI waveguide material. The free spectral range (FSR) is extended to 182 nm and the sharp resonant peaks are obtained. The Young's modulus is determined to be 147.72 GPa and 83.93 GPa under the various applied forces on two directions of SOI material waveguide with the effective mode core area around $A_{eff} =1.0$ μm^2. The proposed method is suitable for measuring Young's modulus of waveguide materials in mirco and nano size with high resolution.

Acknowledgments

References

[1]   F. Rivadulla, M. Banobre-Lopez, C.X. Quintela, A. Pineiro, V. Pardo, D. Baldomir, M.A. Lopez-Quintela, J. Rivas, C.A. Ramos, H. Salva, J.S. Zhou, and J.B. Goodenough, Nature Materials, **9**, 4, pp. 284 (2010).

[2]   B.S. Berry, Dynamic modulus measurements and materials research. Dynamic elastic modulus measurements in materials1990: ASTM special technical. 3-17.

[3]   D.P. Byrne, D. Lacroix, J.A. Planell, D.J. Kelly, and P.J. Prendergast, Biomaterials, **28**, 36, pp. 5544-5554 (2007).

[4]   L. Gong, I.A. Kinloch, R.J. Young, I. Riaz, R. Jalil, and K.S. Novoselov, Advanced Materials, **22**, 24, pp. 2694-2697 (2010).

[5]   J. Cai, R.F. Bie, X.M. Tan, and C. Lu, Physica B-Condensed Matter, **344**, 1-4, pp. 99-102 (2004).

[6]   C.N. Kotanen, F.G. Moussy, S. Carrara, and A. Guiseppi-Elie, Biosensors & Bioelectronics, **35**, 1, pp. 14-26 (2012).

[7]   W. Luo, J.L. Kou, Y. Chen, F. Xu, and Y.Q. Lu, Applied Physics Letters, **101**, 13, pp. (2012).

[8]   A. Martinez-Olmos, S. Capel-Cuevas, N. López-Ruiz, A. Palma, I. De Orbe, and L. Capitán-Vallvey, Sensors and Actuators B: Chemical, **156**, 2, pp. 840-848 (2011).

[9]   C. Sirawattananon, M. Bahadoran, J. Ali, S. Mitatha, and P.P. Yupapin, Nanotechnology, IEEE Transactions on, **11**, 4, pp. 707-712 (2012).

[10]   J. Hu and D. Dai, Photonics Technology Letters, IEEE, **23**, 13, pp. 842-844 (2011).

[11]   S.J. Mason, Proc. IRE, **44**, 9, pp. 920-926 (1956).

[12]   M. Bahadoran, A. Afroozeh, J. Ali, and P.P. Yupapin, Optical Engineering, **51**, 4, pp. 044601-1-044601-8 (2012).

[13]   S. Dey and S. Mandal, Optics Communications, **285**, 4 pp. 439–446 (2011).

[14]   B. Moslehi, J.W. Goodman, M. Tur, and H.J. Shaw, Proceedings of the IEEE, **72**, 7, pp. 909-930 (1984).

[15]   T. Claes, W. Bogaerts, and P. Bienstman, Optics letters, **36**, 17, pp. 3320-3322 (2011).

[16]   S. Dey and S. Mandal, Optics Communications, (2011).

[17]   L. Jin, M. Li, and J.J. He. Highly-sensitive optical sensor using two cascaded-microring resonators with Vernier effect. in Asia Communications and Photonics Conference and Exhibition. 2009. Shanghai, China.

[18]   P. Sanati, A. Afroozeh, I. Amiri, J. Ali, and L.S. Chua, Nanoscience and Nanotechnology Letters, **6**, 3, pp. 221-226 (2014).

[19]   M. Bahadoran, J. Ali, and P.P. Yupapin, Photonics Technology Letters, IEEE, **25**, 15, pp. 1470-1473 (2013).

[20]   S. Mandal, K. Dasgupta, T. Basak, and S. Ghosh, Optics Communications, **264**, 1, pp. 97-104 (2006).

[21]   M. Bahadoran, A.F.A. Noorden, K. Chaudhary, F.S. Mohajer, M.S. Aziz, S. Hashim, J. Ali, and P. Yupapin, Sensors, **14**, 7, pp. 12885-12899 (2014).

[22]   C.K. Madsen and J.H. Zhao, Optical filter design and analysis: a signal processing approach1999: John Wiley & Sons, Inc.

[23]   M. Aziz, S. Daud, M. Bahadoran, J. Ali, and P.P. Yupapin, Journal of Nonlinear Optical Physics & Materials, **21**, 04, pp. (2012).

1104

[24]   S.B. Dey, S. Mandal, and N. Jana, Optik-International Journal for Light and Electron Optics, **124**, 17, pp. 2920-2927 (2013).

[25]   M. Bahadoran, A.F.A. Noorden, K. Chaudhary, S. Aziz, J. Ali, and P. Yupapin, Measurement, (In Press) (2014).

[26]   M. Bahadoran, J. Ali, and P.P. Yupapin, Applied Optics, **52**, 12, pp. 2866-2873 (2013).

[27]   D.G. Rabus, Z. Bian, and A. Shakouri, IEEE Photonics Technology Letters, **17**, 9, pp. 1770 (2005).

[28]   I. Nawi, M. Bahadoran, J. Ali, and P. Yupapin. A Theoretical Model of All-optical Switching Induced by a Soliton Pulse in Nano-waveguide Ring Resonator. in Journal of Physics: Conference Series. 2013. IOP Publishing.

[29]   S. Xiao, M.H. Khan, H. Shen, and M. Qi, Optics express, **15**, 22, pp. 14765-14771 (2007).

[30]   Q. Xu, D. Fattal, and R.G. Beausoleil, Optics express, **16**, 6, pp. 4309-4315 (2008).

[31]   A. Yariv, Electronics Letters, **36**, 4, pp. 321-322 (2000).

[32]   R. Boeck, N.A. Jaeger, N. Rouger, and L. Chrostowski, Optics express, **18**, 24, pp. 25151-25157 (2010).

[33]   T. Wiecek, Composites Part A: Applied Science and Manufacturing, **60**, 1-7 (2014).

[34]   H.-J. Butt, B. Cappella, and M. Kappl, Surface science reports, **59**, 1, pp. 1-152 (2005).